Formation of a necklike structure in $^{35}Cl+^{12}C$ and ^{197}Au reactions at 43 MeV/nucleon

Y. Larochelle, L. Gingras, L. Beaulieu,* X. Qian, Z. Saddiki, B. Djerroud,† D. Doré,‡ R. Laforest,§ R. Roy, M. Samri,‖ and C. St-Pierre
Laboratoire de Physique Nucléaire, Département de Physique, Université Laval, Québec, Canada G1K 7P4

G. C. Ball, D. R. Bowman, A. Galindo-Uribarri, E. Hagberg, and D. Horn
AECL, Chalk River Laboratories, Ontario, Canada K0J 1J0

J. A. López and T. Robinson
Department of Physics, University of Texas at El Paso, El Paso, Texas 79968-0515
(Received 28 August 1996)

The experimental signature of the formation of a necklike structure, with a velocity between that of the projectilelike emitter and that of the targetlike emitter, is investigated with the same beam and experimental setup for targets lighter and heavier than the projectile. The reactions are ^{35}Cl on ^{12}C and on ^{197}Au at 43 MeV/nucleon. Particle velocity distributions are compared with two-source statistical simulations and the presence of a necklike structure is inferred from the data. In the second part of the paper, dynamical model simulations with the formation of a necklike structure are presented for the $^{35}Cl+^{12}C$ system at 43 MeV/nucleon. [S0556-2813(97)01404-0]

PACS number(s): 25.70.Mn, 25.70.Pq

I. INTRODUCTION

There is strong evidence that reaction dynamics plays an important role in the multifragmentation process of heavy ions at intermediate energy [1–9]. In particular, persistence of final-state configurations having a binary character well into the Fermi energy range (10 MeV/nucleon$<E_{\mathrm{beam}}<$100 MeV/nucleon), even for very central or violent collisions, has been confirmed in several recent experiments [10–15]. However, this penomenon still evades proper theoretical explanation. It has been shown that for reactions involving light heavy ions ($Z<20$), the fusion cross section is only 4% or less [14,15] of the total reaction cross section. Another observed phenomenon, still not well understood, is the formation of a necklike structure, recently evidenced in reactions between very heavy ions [16–18] in the Fermi energy range. The concept of a ''neck'' in configuration space between the projectile and the target might be related to the velocity space concepts of midrapidity source, participant-spectator phenomena, or ''fireball'' models commonly used for higher-energy heavy-ion reactions [19–23]. In a study of the Kr + Au reaction at 43 MeV/nucleon, Stuttgé *et al.* [24] concluded, based on velocity distributions, that intermediate-velocity fragments ($Z\geqslant 9$) might come from a participant zone.

In this paper we present experimental evidence for the formation of a necklike structure. The rupture of this neck produces charged particles at velocities between those associated with the projectilelike and targetlike emitters. Two different targets (^{12}C and ^{197}Au) have been used with a ^{35}Cl projectiles at 43 MeV/nucleon in order to assess the similarities between nearly symmetric and very asymmetric systems. In the two cases, noticeable differences have been observed between the experimental results and simulations of the statistical decay of a two-source system.

In the second half of the paper dynamical models such as the Boltzmann-Uehling-Uhlenbeck (BUU) [25] and quantum molecular dynamics (QMD) [6,26] models are briefly introduced and simulations for the $^{35}Cl+^{12}C$ system presented. Although the formation of a necklike structure from dynamical fluctuations is predicted by the QMD model, this process has a very low cross section and most collisions result in compound nucleus formation or deep-inelastic binary systems.

II. EXPERIMENTAL SETUP

The experiment was performed at the Tandem Accelerator SuperConducting Cyclotron (TASCC) at Chalk River. A beam of ^{35}Cl at 43 MeV/nucleon bombarded successively a 2.2 mg/cm^2 thick carbon target and a 2.9 mg/cm^2 gold target. The reaction products were detected in an array of 83 detectors covering polar angles from 3.0° to 46.8°. The 80 detectors of the Laval-Chalk River forward array [27,28] are mounted in five concentric rings around the beam axis and cover nearly 100% of the solid angle between 6.8° and 46.8° (see Fig. 1). The first three rings are made of plastic phoswich detectors with a detection threshold of 7.5 (22.5) MeV/nucleon for $Z=1$ (17) particles. The two outer rings are composed of CsI(Tl) crystals which achieve isotopic resolution for $Z=1$ and 2 ions with a threshold of 2 MeV/

*Present address: M/S 88, Lawrence Berkeley National Laboratory, 1 Cyclotron Road, Berkeley, CA 94720.
†Present address: NSRL, University of Rochester, 271 East River Road, New York 14627.
‡Present address: Institut de Physique Nucléaire d'Orsay, B.P. 91406, Orsay Cedex, France.
§Present address: Cyclotron Institute, Texas A&M, College Station, Texas 77843.
‖Present address: Département de Physique, Faculté des Sciences, Université Ibn Toufail, Kénitra, Maroc.

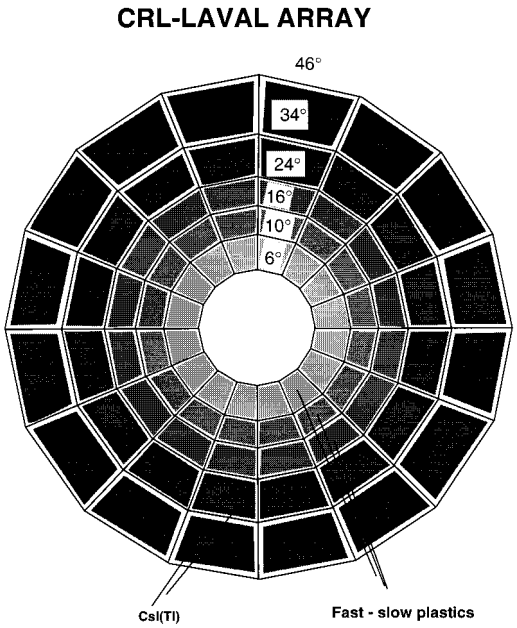

FIG. 1. The CRL-Laval Array. See text for description.

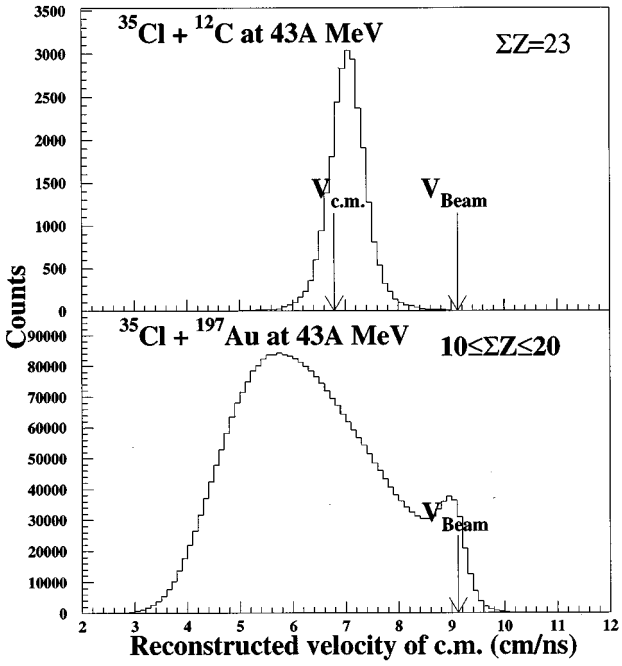

FIG. 2. Reconstructed c.m. velocity from detected ions for events with $\Sigma Z=23$ in ^{35}Cl+ ^{12}C at 43 MeV/nucleon (top) and $10 \leqslant \Sigma Z \leqslant 20$ in ^{35}Cl+ ^{197}Au at 43 MeV/nucleon (bottom). Arrows indicate the beam and c.m. velocity for the reverse kinematics system and the projectile velocity for ^{35}Cl+ ^{197}Au.

nucleon and element identification for $Z=3$ and 4 ions with a threshold of 5 MeV/nucleon. Three Si-CsI telescopes sampled the most forward angles, 3.0°–5.0°, and provided charge identification with a detection threshold of 2 (5) MeV/nucleon for $Z=2$ (17) particles. More details on the experimental setup can be found in Refs. [9,15,29]. Between 10^5 and 10^6 events were recorded for each projectile-target combination in both ''minimum-bias'' and central triggering conditions (charged-particle multiplicities $\geqslant 2$ and $\geqslant 6$, respectively).

Since the effects of the detectors' energy thresholds are different on each system, because of the different system sizes and center-of-mass (c.m.) velocities, a careful selection of events for each experiment must be made before investigating the formation of a necklike structure. Figure 2 shows the c.m. velocity, reconstructed from all detected particles, of the events considered in the present analysis. For the lightest system, ^{35}Cl+ ^{12}C, 2×10^5 events with complete charge detection ($\Sigma Z=23$) are retained. The c.m. velocity distribution of the reconstructed system is narrow and is centered within 4% of the calculated value (this small difference may arise from a combination of minor effects, including preequilibrium emission of target neutrons, an excess of heavy hydrogen isotopes in the phoswich detectors having isotopic identification, systematic calibration uncertainties, and a threshold bias for retaining $\Sigma Z=23$ events with back-angle neutron emission).

In the case of the asymmetric system ^{35}Cl+ ^{197}Au, the array threshold limits contribution from the target to a few light charged particles (LCP's) and the reconstructed c.m. velocity for events with minimum bias ($10 \leqslant \Sigma Z \leqslant 20$) cover a large range, from low values up to the beam velocity. A contribution from the quasielastic scattering of the projectile can be observed at the beam velocity (9.12 cm/ns). However, as shown in Sec. III B, experimental bias does not exclude the detection of LCP's and light intermediate-mass fragment ($Z=3,4$) from a necklike structure for this system.

III. RESULTS AND ANALYSIS

A. ^{35}Cl+ ^{12}C experiment

The presence of charged particles at intermediate velocity in an intermediate-energy heavy-ion reaction should not necessarily be considered as the appearance of a new ''emitting source'' in the system. Rather it can be thought of as a necklike structure formed via both direct nucleon-nucleon interaction and collective mean-field behavior occurring near the c.m. velocity of the system. Charged-particle production could arise from the rupture of such a necklike structure linking the projectilelike emitter (PLE) and the targetlike emitter (TLE).

The presence of a neck in a reaction unveils a ''ternary'' event, where reaction products have three different possible origins: the PLE, the TLE, and the necklike structure. The persistence of the dissipative binary character in the Fermi range and the formation of a necklike structure at c.m. velocity are signs that the incomplete fusion mechanism [30–38] is likely in competition with a nonstatistical mechanism for the production of charged particles.

To extract an experimental signature from a necklike structure, one must first account for the experimental bias of the data. The c.m. velocity of the system is 6.8 cm/ns for ^{35}Cl+ ^{12}C at 43 MeV/nucleon, close to the forward array phoswich thresholds of 5.1 (6.3) cm/ns for $Z=6$ ($Z=12$). Because the energy threshold increases with particle charge, detected heavier fragments are likely to be faster on average than lighter ones. In order to properly assess threshold effects and to avoid experimental artifacts, every experimental distribution will be compared to simulations from the code EUGENE [39], filtered for both the detector's energy threshold and geometry. This code produces two-source events that are

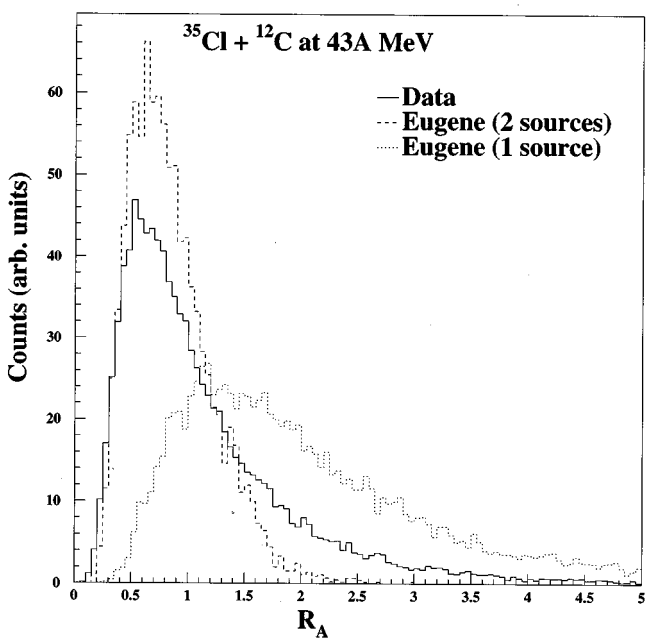

FIG. 3. Anisotropy ratio for ^{35}Cl+ ^{12}C (solid line) and EUGENE one- and two-source simulations (dotted and dashed lines, respectively) with no selection on flow angle.

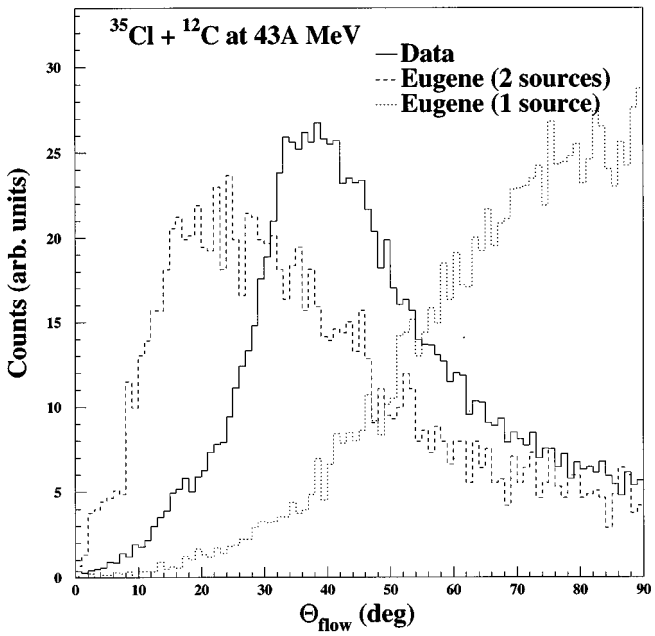

FIG. 4. $\Theta_{\rm flow}$ distribution for the ^{35}Cl+ ^{12}C at 43 MeV/nucleon (solid line). Dotted and dashed lines are from filtered one- and two-source EUGENE simulations, respectively.

realistic in kinematics, excitation energy (equal temperature limit approximation), and angular momentum sharing between the nuclei. Complete fusion is predicted for small impact parameters, allowing the treatment of single- and two-source simulations with the same code.

As in previous analyses [9,13,15], the anisotropy ratio [40] is used to compare data and simulations that have the same elongation in the momentum space. This anisotropy ratio is defined as

$$R_A=\frac{2}{\pi}\frac{\Sigma_{i=1}^{M}|P_{i\rm c.m.\perp}|}{\Sigma_{i=1}^{M}|P_{i\rm c.m.\parallel}|}, \tag{1}$$

where $2/\pi$ is a geometric normalization constant, M is the charged-particle multiplicity, and $P_{i\rm c.m.\parallel}$ and $P_{i\rm c.m.\perp}$ are momenta of the ith particle in the c.m. frame, parallel and perpendicular to the beam axis. Figure 3 shows that in order to reproduce the anisotropy distribution of the $\Sigma Z=23$ data in ^{35}Cl+ ^{12}C at 43 MeV/nucleon, EUGENE simulations of two-source events with an impact parameter of 4.0 fm or greater are required. Single-source events have on the average a mean value of anisotropy ratio higher than that of the data.

As shown in Refs. [14,15] for light systems, a small portion ($\leqslant 5\%$) of the reaction cross section in this energy range leads to single-source events. It is important to separate those events from the data before making a comparison to binary simulations. To do so an event-shape tensor analysis was performed using the quadratic momentum tensor [41]:

$$P_{i,j}^2=\Sigma_{n=1}^{N_{\rm CP}}P_i^{(n)}P_j^{(n)}, \quad i,j=1,2,3, \tag{2}$$

where $P_i^{(n)}$ and $P_j^{(n)}$ are the ith or jth Cartesian c.m. components of the particle momentum and $N_{\rm CP}$ is the total number of charged particles in the event. The three eigenvalues and eigenvectors calculated from this tensor define the shape of the event. The angle between the major axis of the event in momentum space (the eigenvector with the largest eigenvalue) and the beam axis is $\Theta_{\rm flow}$, the flow angle.

Figure 4 shows the experimental flow angle distributions for the ^{35}Cl+ ^{12}C system and corresponding one- and two-source simulations. Based on perpendicular versus parallel velocity spectra, it has been demonstrated in Ref. [15] that a cut on the flow angle is a better criterion than transverse energy for isolating binary (or ternary) events. Furthermore, distributions of flow angle for simulated single-source events plotted in the figure show that a majority of these events do correspond to the highest values of $\Theta_{\rm flow}$. The $Z=3$ perpendicular versus parallel velocity spectra for specific ranges of the flow angle are shown in Fig. 5 for ^{35}Cl+ ^{12}C, where the cut for binary events is set at $\Theta_{\rm flow}<45°$ and at $\Theta_{\rm flow}>65°$ for single-source events. It is clear from the velocity maps that the two-source events are selected by the cut on $\Theta_{\rm flow}<45°$ and that single-source events, where the $Z=3$ emission is isotropic in the center of mass, are largely eliminated. The one-source and two-source EUGENE simulations, also plotted in the figure, support that selection since most of the two-source events, where the emitters are well separated, are found within the $\Theta_{\rm flow}<45°$ cut and the isotropic one-source events within the $\Theta_{\rm flow}>65°$ cut.

For the remainder of the analysis we use events with $\Theta_{\rm flow}<45°$, corresponding to the events with a binary (or ternary) nature, where a necklike structure is most likely to appear. The contribution from one-source events in the experimental data should be negligible because of this cut on $\Theta_{\rm flow}$. The contribution of one-source events to the individual-particle velocity spectra can be estimated to be at most 5% of detected events with $\Theta_{\rm flow}<45°$. This is done by comparing the total yield and the yield at 90° of the flow angle distributions for the data and the one-source simulation. Also, a necklike structure would be better characterized kinematically by charged particles with $2\leqslant Z\leqslant 9$ [hereafter

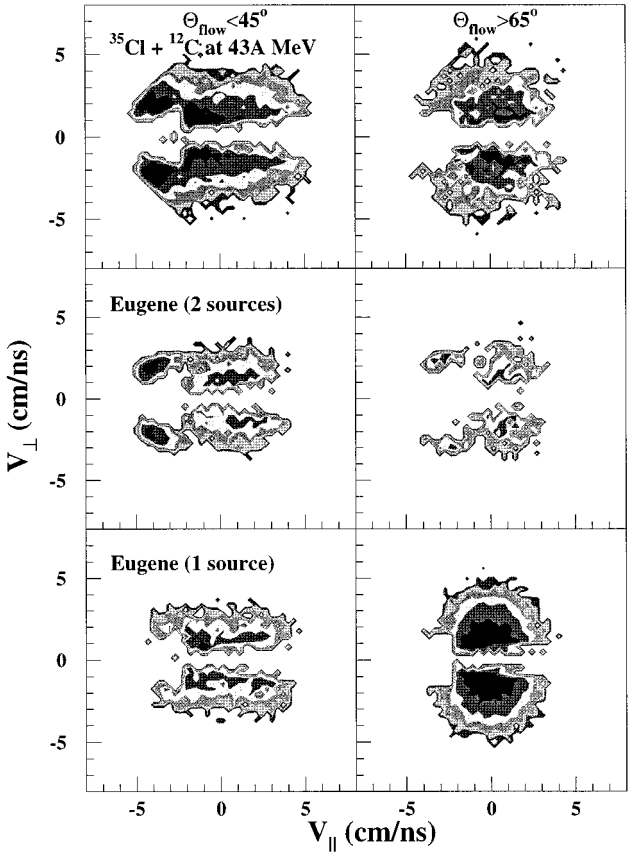

FIG. 5. Galilean-invariant yields of $Z=3$ fragments from the $^{35}Cl+^{12}C$ at 43 MeV/nucleon system (top panels) and filtered one- (middle panels) and two- (bottom panels) source EUGENE simulations plotted as a function of perpendicular versus parallel velocity in the c.m. frame, with cuts on $\Theta_{flow}<45°$ (left panels) and $\Theta_{flow}>65°$ (right panels). Parallel velocities are along the beam axis. The count yield is in a logarithmic scale.

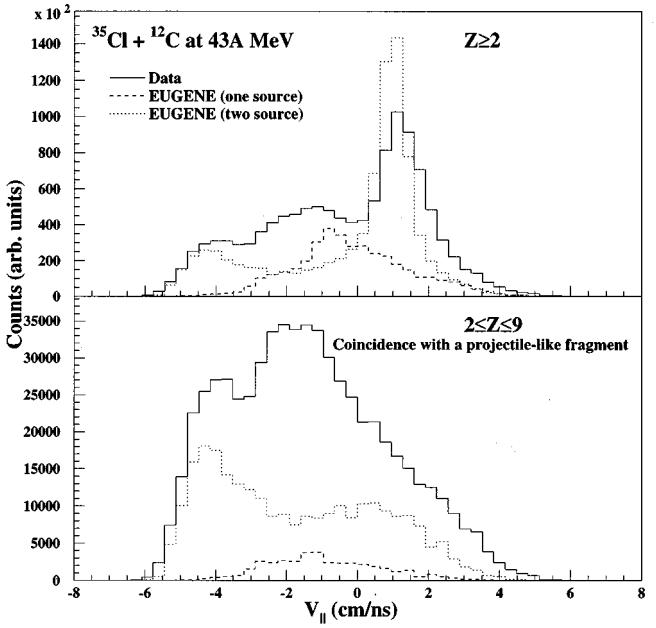

FIG. 6. Parallel velocity distribution of all particles with $Z\geq 2$ for events with $\Theta_{flow}<45°$ for the $^{35}Cl+^{12}C$ at 43 MeV/nucleon system (top panel) for data (solid line), and EUGENE one-source (dashed line) and two-source simulations (dotted line). The same number of events was used for the three distributions. The bottom panel shows the parallel velocity distribution for particles with $2\leq Z\leq 9$ that are in coincidence with a projectilelike fragment (defined as a fragment with $Z\geq 6$ and parallel velocity $\geq$ 0.5 cm/ns in the laboratory c.m. frame).

defined as CP(2–9)], because the protons may be linked to prethermalization processes [30,37,42–45] and the heaviest ions are mainly residues from the PLE. Our analysis therefore focuses on these particles.

The longitudinal component of the velocity in the center-of-mass system is shown in the top panel of Fig. 6 for all $Z\geq 2$ products of 20 000 measured $^{35}Cl+^{12}C$ events (solid line). The same number of simulated one-source and two-source events generated with the code EUGENE is shown as dashed and dotted lines, respectively. This represents the two extreme cases in which the charged-particle velocity distributions come entirely from one-source events or entirely from two-source events. Only events with $\Theta_{flow}<45°$ are used in the velocity distributions. In addition to the targetlike and projectilelike velocity components, at -4 and 1 cm/ns in the figure, an intermediate-velocity component is visible in the data between -3 and 0 cm/ns. While it might seem reasonable to attribute the three-component structure in the data to a superposition of one-source and two-source events, an analysis of coincidence data eliminates this possibility. The lower panel of the figure shows the velocity distributions, from the same events, of all CP(2–9) coincident with projectilelike fragments ($Z\geq 6$, $v_{c.m.\|}\geq 0.5$ cm/ns). This definition is based on the evaporation residue charge distribution of the EUGENE simulations, which both have a mean value of $Z=8$. The intermediate-velocity peak remains in coincidence with projectilelike fragments; single-source events are less likely to have a high-velocity heavy fragment and the resulting simulated coincidence spectrum (dashed line) is not strong enough to account for the intermediate-velocity component. This conclusion is corroborated by the fact that the contribution of one-source events in the data has been estimated (see above) to be at most 5% of the events with $\Theta_{flow}<45°$. The simulated two-source coincidence spectrum remains forward (≥ 0 cm/ns) and backward (≤ -3 cm/ns) peaked. The three-peak structure of the top panel must therefore originate from three-component events rather than from a summing of separate fusion and binary reactions.

To assess the difference between binary and ternary events, we inspect the perpendicular and parallel velocity distributions of the particles. In order to find the kinematic origin of the charged particles emitted during the reaction, an exclusive analysis is performed based on the heaviest particles of each event. Results from filtered EUGENE two-source simulations indicate that detected particles originating from the TLE are mostly found in CsI(Tl) detectors (between 24° and 47° in the laboratory). Most of those coming from the PLE are found in the plastic phoswich array and Si-CsI telescopes (together covering angles between 3° and 24°). Based on these results, the following method is used to probe the origin of charged particles: The two ''forward'' heaviest particles (detected in phoswiches or telescopes) and the heaviest one emitted ''backward'' in the center-of-mass frame [i.e., detected in the CsI(Tl) array] were identified for each event. Individual and total velocity distributions of

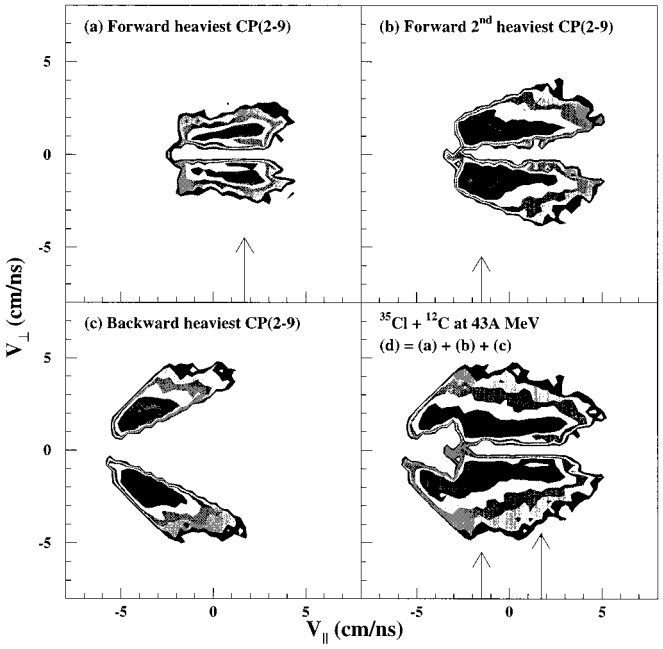

FIG. 7. Galilean-invariant perpendicular versus parallel velocity spectra of charged particles ($2 \leqslant Z \leqslant 9$) in the c.m. frame for the ^{35}Cl+^{12}C at 43 MeV/nucleon system with $\Theta_{\text{flow}} < 45°$ for the heaviest (top left) and second heaviest (top right) ions detected in the phoswich detectors and for the heaviest ions detected in the CsI(Tl) scintillators (bottom left). The total of the three distributions is shown in the bottom right panel. Parallel velocities are along the beam axis and the count yield is in a logarithmic scale. Arrows shows the peak of the distributions for the heaviest and second-heaviest charged particle.

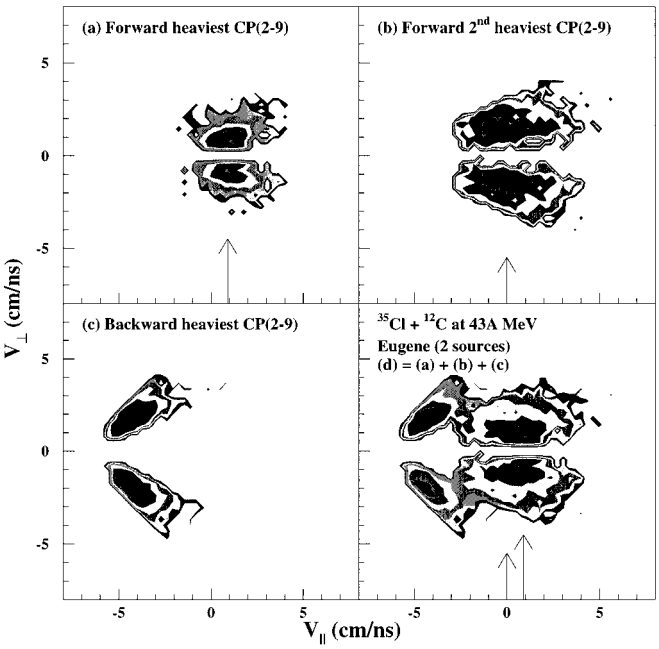

FIG. 8. Same as Fig. 7 but for EUGENE two-source simulations of ^{35}Cl+^{12}C at 43 MeV/nucleon with $b > 4.0$ fm and with $\Theta_{\text{flow}} < 45°$.

these three groups of charged particles are presented in Fig. 7 for the ^{35}Cl+^{12}C system. Only CP(2–9) are plotted in the figure. It should be noted that the forward heaviest CP(2–9) travels with an average velocity of 1.7 cm/ns (in the c.m. reference frame). There is a major contribution of the second-heaviest forward CP(2–9) particle, found near the c.m. velocity (-1.5 cm/ns). The maxima of the heaviest and second-heaviest charged-particle velocity distributions are separated by ≈ 3 cm/ns. The backward heaviest CP(2–9) has an average velocity of -4 cm/ns. The overall velocity map of the three heaviest charged particles, panel (d), shows a smooth distribution pattern between -4 and $+4$ cm/ns.

The second-heaviest CP(2–9) observed could be slower, simply because the phoswich energy threshold increases with the charge. To evaluate the magnitude of this bias, a comparison is made to two-source simulations analyzed in the same way as the data. Figure 8 shows the same velocity distributions as Fig. 7, but for the filtered ^{35}Cl+^{12}C EUGENE two-source simulation. Here, the average velocity of the forward heaviest CP(2–9) is estimated at 0.9 cm/ns. This is a lower value than the 1.7 cm/ns of the data. This shows that the kinematic damping of the PLE is overestimated in the binary simulation even though the momentum anisotropy of the data is well reproduced by the simulations, as shown in Fig. 3. Similar conclusions on damping were reached recently by Dempsey *et al.* [46] for heavier systems. The difference in velocity between the heaviest and second-heaviest CP(2–9) is of the order of 1 cm/ns, compared to 3 cm/ns in the data. This difference is due in part to the higher threshold for heavier ions, but since the difference in the data is nearly 3 times larger, an important intermediate-velocity (neck) contribution to the velocity maps has to be considered. Also, there is a depletion between the heaviest and backward heaviest CP(2–9), in sharp contrast with the continuous pattern of the experimental data. These differences with the data would be explained by the presence of a faster and lighter PLE in the data and the formation of a necklike structure traveling near the c.m. velocity.

B. ^{35}Cl+ ^{197}Au experiment

For an asymmetric collision of a light projectile with a heavy target, the analysis must be done differently, mainly because the energy threshold of the experimental apparatus only permits the detection of projectile residues and of fast light particles from the target. While the formation of a necklike structure in such an asymmetric system has never been observed directly, the signature of intermediate-velocity emission in low-Z energy spectra at large angles and ''quasifree nucleon knockout'' at more forward angles has been presented by Awes *et al.* [47] for the ^{16}O+Au system. This model failed to reproduce data for a more symmetric system. Even with thresholdless detectors, the kinematics involved in a very asymmetric collision makes it difficult to select particles emitted from a necklike structure since the c.m. velocity of the system would be extremely close to the target velocity. However, the intermediate-velocity emitter identified in asymmetric collisions was often found to be close to half the projectile velocity [7], even in the intermediate-energy range of our experiment [48], leading to the conclu-

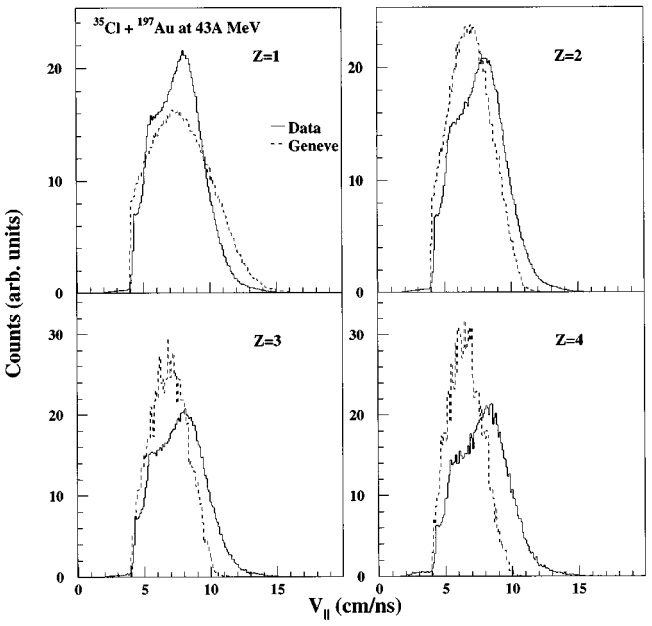

FIG. 9. Parallel velocity distributions for $Z=1$ (top left), 2 (top right), 3 (bottom left), and 4 (bottom right) from the ^{35}Cl+ ^{197}Au system at 43 MeV/nucleon with $10 \leqslant \Sigma Z$ (detected) $\leqslant 20$. Solid lines are for data, dashed lines for two-source GENEVE simulations.

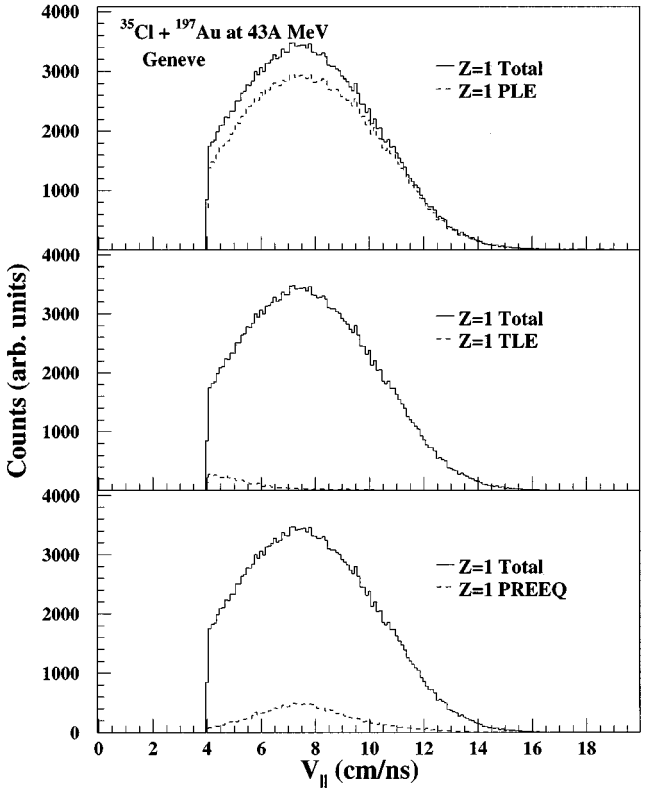

FIG. 10. Parallel velocity distributions for $Z=1$ from the PLE (dashed line, top panel), TLE (dashed line, middle panel), and preequilibrium emission (dashed line, bottom panel) compared to the total distribution (solid lines) predicted by two-source GENEVE simulations with $10 \leqslant \Sigma Z$ (detected) $\leqslant 20$.

sion that this intermediate system could be formed by nucleon-nucleon scattering between the projectile and the target [49].

For the analysis of the ^{35}Cl+ ^{197}Au reaction at 43*A* MeV, the code GENEVE [50] was used for comparison with the data instead of EUGENE. It also evaluates the early stage of the reaction with respect to excitation energy sharing and angular momentum, but it has provisions to include projectilelike and targetlike preequilibrium emission of protons and neutrons. In the dissipation stage, at small impact parameters, the code assumes a complete damping of the initial relative motion between the two nuclei and the formation of a thermalized compound nucleus (incomplete fusion). For larger impact parameters, the excitation energy is shared between the PLE and the TLE, according to their relative masses. The deexcitation phase is similar to that followed by the code EUGENE. Simulations leading to incomplete fusion were not retained for the present analysis. For both the data and the simulations the only event selection criterion was that at least 10 units of charge were detected. The reconstructed c.m. velocity of filtered GENEVE events cover a range of values as large (from 4 to 9 cm/ns) as in the data.

In Fig. 9, the distributions of velocity parallel to the beam in the laboratory reference frame for particles with $Z=1$, 2, 3, and 4 are compared to filtered GENEVE projectile breakup simulations. The main characteristic of the spectra is the ''shoulder'' present in the data below the main peak of the distributions seen above the detector threshold and absent in the simulations. These ''shoulders'' in the lower part of the light-particle and IMF velocity spectra were observed in other projectile breakup analysis done with completely different experimental setups [51,52], and were not attributed as a contribution from the heavy target. Also interesting is the difference between the experimental peak position and that from binary simulations. The experimental maximum is at a systematically higher velocity, especially for the heavier $Z=3$ and $Z=4$ particles, indicating a faster velocity for the PLE. The same trend had been observed for the lighter nearly symmetric system detailed in the last section.

Nucleon-nucleon scattering at midrapidity could produce LCP at the c.m. velocity, but not the heavier charged particles. On the other hand, the trend in the data is compatible with the formation of a necklike structure, resulting in a greater kinematic separation between the PLE and TLE or, in this case, the light PLE and the heavy target.

To further explore the effects of detector bias and the contribution from the target and/or preequilibrium emission to the velocity spectra, Fig. 10 shows the filtered GENEVE $Z=1$ parallel velocity distribution and the relative contribution from the PLE (top panel), TLE (middle panel), and projectilelike preequilibrium (bottom panel). From these plots, it can be concluded that the experimentally observed shoulders do not arise from either TLE or from preequilibrium LCP emission, which is centered on the PLE velocity. This represents additional evidence of the formation of a necklike structure due to the neutron-rich nature of the heavy target in the asymmetric ^{35}Cl+ ^{197}Au reaction.

This effect is even stronger when isotopic ratios outside the normal emission range of the PLE are examined. Based on systematics put forward by Lleres *et al.* [53] to isolate the PLE, the emission range of an excited ^{35}Cl is set at $+/-4$ cm/ns around the PLE residue. Figure 11 shows the proton, deuteron, and triton ratios to the corresponding total number of hydrogens for parallel velocities lower and higher than 4

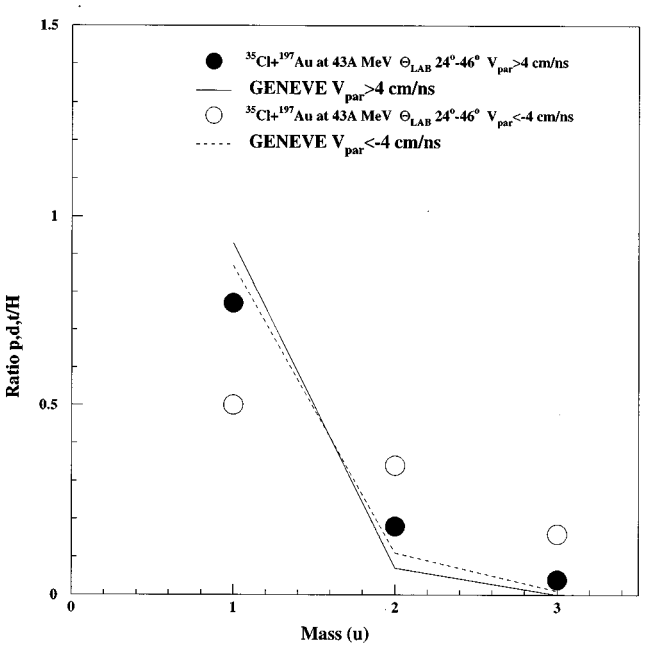

FIG. 11. Ratio of protons (mass=1), deuterons (mass=2), and tritons (mass=3) to the respective total number of hydrogens emitted forward of 4 cm/ns and backward of −4 cm/ns (see text for details). Data are represented by solid dots for forward emission and open dots for backward emission and the GENEVE simulation by a solid line for forward emission and a dashed line for backward emission.

cm/ns to that of the heavy PLE residue. The ratio distribution for forward emission is well reproduced by GENEVE simulations. However, although there is a small change in the simulation, the backward ratios are dramatically different for the experimental data, showing many more neutron-rich deuterons and tritons.

This is further evidence for the formation of a necklike structure, richer in neutrons than the PLE because of a contribution to its composition from the neutron-rich target.

IV. DYNAMICAL SIMULATIONS

Statistical codes such as EUGENE and GENEVE (and the combinations of TORINO [54] with GEMINI [55] or SOS [56] as used in Refs. [9,13]) are based on excitation mechanisms involving nucleon exchange or excitation energy sharing as a function of the impact parameter and on sequential evaporation of a statistical nature. Moreover, they do not predict the formation of a necklike structure, as shown in the previous section. In this section, we analyze different dynamical calculations which could shed some light on the experimental results, especially on the persistence of binary dynamics and the formation of a necklike structure.

Boltzmann-Uehling-Uhlenbeck (BUU) and quantum molecular dynamics (QMD) models are frequently used to describe heavy-ion collisions at intermediate energy. The BUU model [25] is based on one-body theory, which is described in the model by a calculation of the one-body phase-space density function. However, it is difficult to treat correlations and fragmentation in heavy-ion collisions with the BUU model. The QMD model [26] incorporates the important quantum features of BUU theory, explicitly treating the nucleon correlation information through the time evolution of the collision. It is able to describe the fluctuations that lead to the final fragmentation of the nuclear system. This is a major improvement over the BUU model. The QMD model is quite successful in describing collective effects such as bounce-off and squeeze-out. However, it fails in reproducing the fragment multiplicities observed experimentally. Nevertheless, the QMD and BUU models describe the initial nonequilibrium stage of the collision in reasonable detail and should predict the prethermalization nucleon emission and the formation of highly excited prefragments.

To investigate the persistence of a binary character, even for central collisions, and the formation of intermediate-velocity neck in light heavy-ion collisions, we have performed BUU calculations for ^{35}Cl+ ^{12}C at 43 MeV/nucleon. The BUU equation has been solved with the parallel ensemble method [57]:

$$\frac{\partial f_1}{\partial t} + v \cdot \nabla_r f_1 - \nabla_r U \cdot \nabla_p f_1$$

$$= \frac{4}{(2\pi)^3} \int d^3k_2 d\Omega \frac{d\sigma_{nn}}{d\Omega} v_{12} [f_3 f_4 (1-f_1)(1-f_2) - f_1 f_2 (1-f_3)(1-f_4)]. \quad (3)$$

In Eq. (2), $f=f(r,p,t)$ is the Wigner transformation of the one-body density matrix, $d\sigma_{nn}/d\Omega$ and v_{12} are the in-medium cross section and the relative velocity for the colliding nucleons, respectively, and U is the total mean-field potential which consists of the Coulomb potential and the nuclear potential with isoscalar and symmetry terms. During our calculations, we used parameters for the equation of state (EOS) which correspond to values of nuclear compressibility at $K=380$ MeV (stiff EOS). For simplicity, $\sigma_{nn}(\theta,\phi)$ is chosen to be isotropic and energy independent. The mean-field and the Pauli-blocking factors in the collision integral are averaged over an ensemble of 200 parallel simulations.

Figure 12 shows the time evolution of density profiles on the reaction plane for three impact parameters with a BUU model. For the calculation at $b=3.0$ fm, a single deformed residue is still present at $t=220$ fm/c. In contrast, the separated projectilelike and targetlike fragments begin to show at slightly larger impact parameter $b=3.5$ fm and become distinct at $b=4.0$ fm. So, in this calculation, the critical impact parameter is 3.5 fm for the transition from the one-body to the two-body process. However, the calculation cannot produce neck fragments or a necklike structure in semiperipheral collisions (between 2 and 4 fm). BUU simulations using a lower value of nuclear compressibility (soft EOS) were similar.

Recently, Sobotka [58] has performed BUU calculations for the ^{136}Xe+ ^{208}Bi system at 28 MeV/nucleon considering a simple asymmetry-dependent term in the potentials which conspired to create reasonable neutron ''skins'' for heavy nuclei. Compared to calculations done with more commonly used equation of state, the calculations produced neutron-rich neck regions with higher probability. Neutron skin effects were shown to be a possible origin of necklike structure in heavier systems. These effects cannot be considered in ''neutron-poor'' systems such as ^{35}Cl+ ^{12}C studied here. A

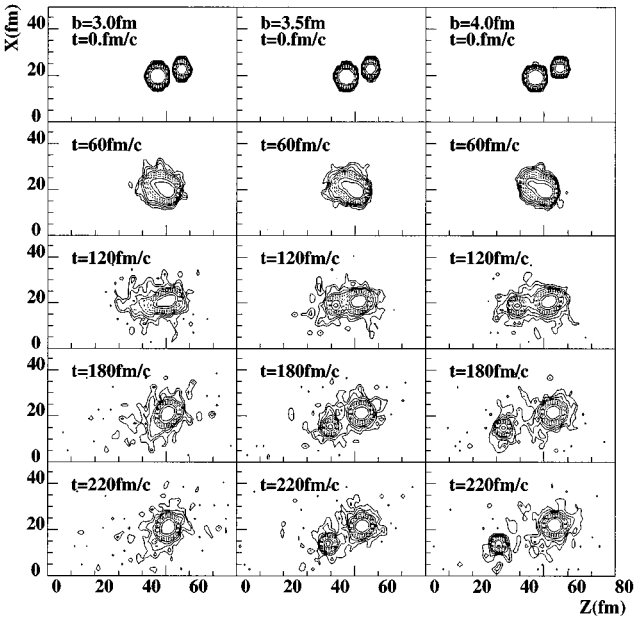

FIG. 12. Time evolution of density profiles on the reaction plane for ^{35}Cl+^{12}C at 43 MeV/nucleon reaction, at three impact parameters calculated with the BUU model (unfiltered).

possible origin of necklike structure for light heavy-ion systems is dynamical fluctuations. Colonna *et al.* [59] have implemented a fluctuating term into the BUU equation, arising from consideration of the random nature of the nucleon-nucleon collision integral. Their calculations predicted the existence of an intermediate neck region and the direct emission of intermediate mass fragments from the region.

To study the important role of mean-field instabilities which originate from dynamical fluctuations in the reaction dynamics, we have performed QMD calculations for the ^{35}Cl+^{12}C system at 43 MeV/nucleon. Details about the code may be found in Ref. [60]. Here we summarize briefly the relevant properties. In the model, each nucleon of two colliding nuclei is described by a Gaussian in momentum and coordinate space:

$$f_i(r,p,t)=\frac{1}{(\pi\hbar)^3}\exp\left\{-\frac{[r-r_{i0}(t)]^2}{2L}-[p-p_{i0}(t)]^2\frac{2L}{\hbar^2}\right\}, \tag{4}$$

where r_{i0} and p_{i0} are the centroids of the ith particle in coordinate and momentum space and $2L$ is the characteristic width of the wave packet. The nucleons interact via a potential during the collision. The interaction used here consists of a local Skyrme two- and three-particle interaction, a Coulomb interaction, and a Yukawa interaction. Neutrons and protons are distinguished in the interaction.

With these Gaussian nucleon distributions, the interactions lead to the following Hamiltonian:

$$H=\sum_i \frac{p_i^2}{2m}+V^{\rm loc}+V^{\rm Yuk}+V^{\rm Coul}. \tag{5}$$

The short-range interaction is taken into account in the same way as in the BUU models via a stochastic scattering term: Two nucleons can scatter if the spatial distance of the centroids of their Gaussians is smaller than $\sqrt{\sigma_{\rm tot}/\pi}$. The free nucleon-nucleon cross section is modified in the medium by the Uehling-Uhlenbeck blocking factors. The Pauli blocking probability of the final states is determined by the overlap of the two nucleons in phase space with all other nucleons. If a collision is blocked, the momenta of the scattering parameters prior to the scattering are restored. We define the fragments at the end of the reaction using a common minimum spanning tree procedure. If the centroids of their wave packets have a spatial relationship $d_0 \leqslant 3$ fm, two nucleons are considered to be bound in a fragment.

For the nuclear ground state, Fermi motion generated by the Pauli exclusion principle has been simulated by a momentum-dependent repulsive potential. The parametrized Gaussian Pauli potential [61] is defined as

$$E_{\rm Pau}=\frac{1}{2}\sum_{i\neq j} V_{\rm Pau}^0\left[\frac{\hbar}{q_0p_0}\right]^2\exp\left[-\frac{r_{ij}^2}{2q_0^2}-\frac{p_{ij}^2}{2p_0^2}\right]\delta_{\tau_i\tau_j}\delta_{\sigma_i\sigma_j}, \tag{6}$$

where σ_i and τ_i denote the spin and isospin index of nucleon i. With such a potential the total energy of the ''free'' Fermi gas is given by $E_{\rm tot}^{\rm FG}=E_{\rm kin}+E_{\rm Pau}$. The parameters for the equation of state (EOS) and Pauli potential used in the calculation are taken from Ref. [62], which correspond to a stiff EOS parameter of $K=380$ MeV.

The implementation of the Pauli potential into the dynamical QMD model yields two major improvements relative to earlier models [62]. First, the ground states are well defined; this yields stable initial nuclei. This is very important for QMD model to be used in the Fermi energy region, $E_{\rm lab}\approx 30$ MeV/nucleon [63,64]. Second, the excitation energy of the prefragments can be determined with respect to the true ground state and used to describe the long-term behavior of those fragments in an independent model such as a statistical decay model.

For a systematic study, we generated several thousand events, with the number of events contained in a given domain of impact parameter proportional to the cross section. For each time step, the momenta and the position of all nucleons were stored and the spatial distribution of the nucleons was investigated to examine the formation of the fragments.

After the collision has taken place, the system will continue to emit particles both in the prethermalization and the quasithermalization processes. Therefore the masses and excitation energies of prefragments are sensitive to the freeze-out time at which observables are evaluated. During the calculation, we switched off the QMD calculations at a time of 120 fm/c after the first contact of two colliding nuclei (at $t=0$ the projectile and target surfaces are separated by approximately 2.0 fm). At this time the fast prethermalization processes are terminated (the time for prethermalization emission is nearly 70 fm/c) and the mass and excitation energies of the prefragments do not change rapidly with time, which can be seen as evidence that the nuclear system is approaching thermal equilibrium before breakup.

Figure 13 shows the impact parameter b versus mass distribution of prefragments for ^{35}Cl+^{12}C at the 43 MeV/nucleon reaction with QMD calculations at $t=120$ fm/c. In

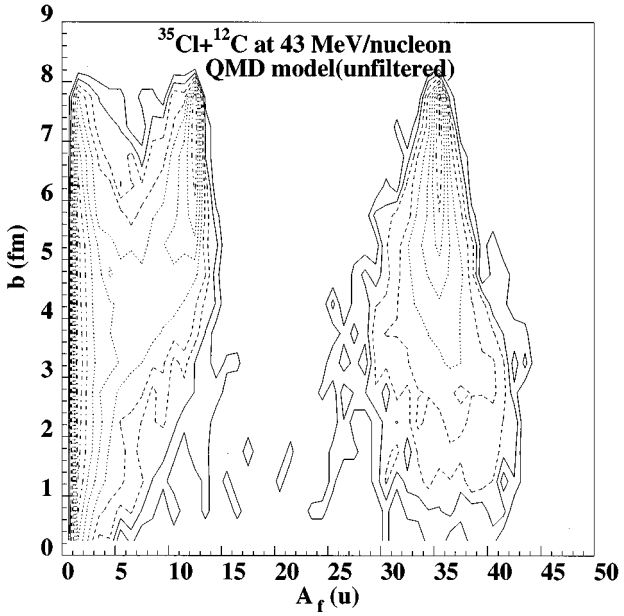

FIG. 13. The mass distribution for prefragment emission, plotted against impact parameter b for ^{35}Cl+ ^{12}C at 43 MeV/nucleon reaction at $t=120$ fm/c with QMD calculation (unfiltered). Each contour represents a factor slightly higher than 2.

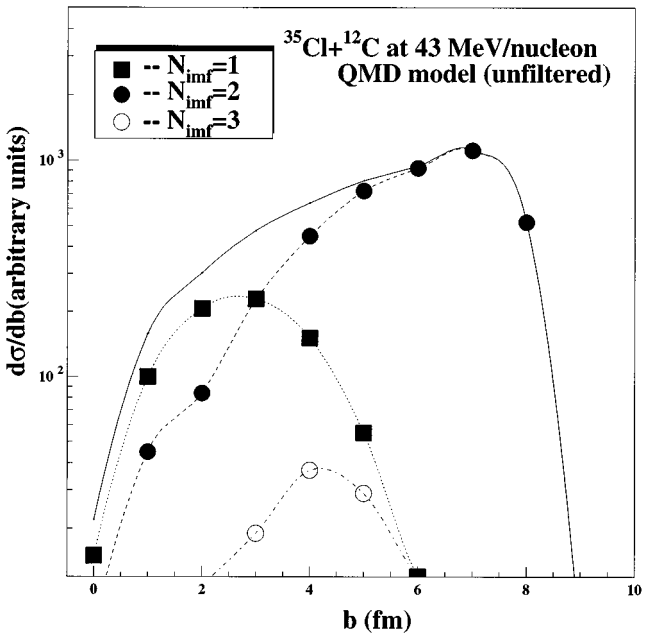

FIG. 14. Unfiltered QMD calculation of the differential cross section $d\sigma/db$ for the production of one, two, and three IMF's plotted against impact parameters b for the ^{35}Cl+ ^{12}C reaction at 43 MeV/nucleon at $t=120$ fm/c. The solid line represents the impact parameters distribution used in the simulation.

the case of a head-on collision, we see that the fragment mass distribution is composed of a heavy residue $A_f \approx 41$ and a few nucleons. In the semiperipheral region $b \approx 3.5$ fm, heavier prefragments appear, possibly leading to IMF production. For the peripheral region, $b \geq 6.0$ fm, we see clearly that the fragment mass distribution is composed of heavy fragments of $A_f \approx 34$ and $A_f \approx 10$, respectively, along with nucleons.

From an event-by-event analysis of the simulation we can correlate the number of produced prefragments to the impact parameter. In the case of a central collision, only one heavy fragment is produced. This means that the reaction mechanism is complete or incomplete fusion. With a slight increase of impact parameter, in addition to the incomplete fusion process, we can observe two-fragment events in the midcentral region. From the time evolution of the spatial distribution of nucleons, we observe such events originating from an incompletely fused system reseparated into two fragments, from which nucleons and/or clusters continue to escape. In the semiperipheral region, around 3.5 fm, in addition to one- and two-fragment events, we also observe a small cross section of three-fragment events. As stated above, for peripheral collisions, $b \geq 6.0$ fm, two heavy prefragments are formed, which could be attributed to a targetlike fragment (TLF) and a projectilelike fragment (PLF). Here, the collision process is just a dissipative binary process as in deep-inelastic collisions.

In Fig. 14, we show the differential cross section $d\sigma/db$ for one, two, and three IMF's as a function of impact parameter b for ^{35}Cl+ ^{12}C reaction at 43 MeV/nucleon as predicted from our QMD calculations. The IMF's are defined here as prefragments with $Z \geq 3$. The cross section of 1 IMF events, which approximately correspond to the incomplete fusion at small impact parameter, is 15% of the reaction cross section. It is still larger than the 4% from experimental results [15]. Dissipative binary collisions (2 IMF events) are the dominant reaction process; they account for about 80% of the cross section and occur almost at all impact parameters, even in central collisions. The cross section for 3 IMF events is only of the order of 3% of the cross section. At $b=3.5$ fm, the cross section of 1 IMF events is equal to that of 2 IMF events. This prediction is consistent with the BUU calculations.

To search for the formation of a necklike structure, we produced a contour plot of the IMF velocity components (v_z) versus position z on beam direction for 3 IMF events, as shown in Fig. 15. An interesting result is that the IMF can be classified into three groups. A first group is in the region of $z \geq 0$ fm and $v_z \geq 1.0$ cm/ns, representing fragments with a mass $A_f \approx 31$, and it could be attributed to the PLF. A second group is in the region of $z \leq -15$ fm and $v_z \leq -3.0$ cm/ns, $A_f \approx 7$, and could be attributed to the TLF. For the remaining group, its velocity is near to -0.5 fm/c, $z \approx -5$ fm, and $A_f \approx 7$. Because its character is similar to what is called the participant-spectator process in higher-energy heavy-ion collisions, we consider it as a necklike structure. It is concentrated in midperipheral collisions as shown in Fig. 14. In summary, the BUU model fails to yield any indication of an intermediate-velocity IMF production, while QMD does appear to predict a small such component.

V. CONCLUSION

We have investigated the formation of a necklike structure in intermediate-energy reactions involving ''light'' heavy ions. For the reverse-kinematics system (^{35}Cl+ ^{12}C), the presence of necklike structure is observed by two different methods: coincidences with a projectilelike fragment and

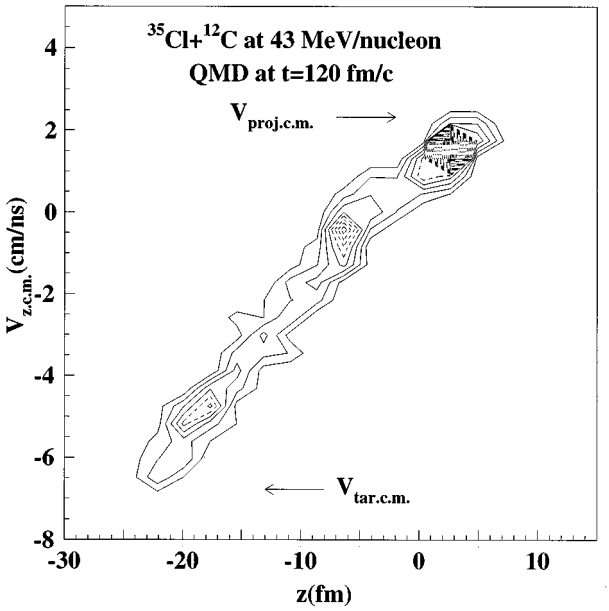

FIG. 15. Unfiltered QMD calculation of the IMF velocity components (v_z) versus position components z on the beam direction (z axis) for 3 IMF events in the $^{35}Cl+^{12}C$ reaction at 43 MeV/nucleon at $t=120$ fm/c.

relative velocities between the two heaviest charged particles, in comparison with filtered two-source simulations. The kinematic damping of the PLE is also overestimated in the binary simulations even though the anisotropy of the events is well reproduced. For the heavier nuclear system ($^{35}Cl+^{197}Au$), the appearance of a necklike structure has also been observed in the velocity distributions of LCP's and light ions and in the isotopic ratio of $Z=1$ particles. For this very asymmetric system, however, a clear signature of the formation of a necklike structure would require detection of the target residue.

We have performed BUU and QMD calculations for the reaction $^{35}Cl+^{12}C$ at 43 MeV/nucleon. With our choice of input parameters, BUU calculations give a critical impact parameter of 3.5 fm for the transition from a one-body to a two-body process. The model cannot produce necklike structures in semiperipheral collisions as observed in the experimental results. QMD calculations which preserve dynamical fluctuations through the time evolution of the collision can produce necklike structures at $b\approx 4$ fm for the $^{35}Cl+^{12}C$ reaction. With the QMD model, the most probable origin of a necklike structure for light heavy-ion system lies in dynamical fluctuations. The calculated cross section for necklike structure events is less than 3% of cross section at 43 MeV/nucleon. For the systems studied, the calculations predict that binary dissipative collisions are a dominant reaction process, occurring over a large range of impact parameters and, even, in central collisions.

Results from more complete experiments, possibly including complete isotopic resolution, and more detailed dynamical simulations are needed before the mechanisms can be definitively identified. However, it is evident from our results that along with statistical mechanisms, reaction dynamics, specifically neck rupture, plays a major role in the production mechanism of charged particles.

ACKNOWLEDGMENTS

We would like to thank D. Durand and J.-P. Wieleczko for the use of their statistical codes, G. Peilert for the QMD code, and W. Bauer for the BUU code. This work was supported in part by the Natural Sciences and Engineering Research Council of Canada and the Fonds pour la Formation de Chercheurs et l'Aide à la Recherche.

[1] D. Jouan, B. Borderie, M.F. Rivet, C. Cabot, H. Fuchs, H. Gauvin, C. Grégoire, F. Hanappe, D. Gardes, M. Montoya, B. Remaud, and F. Sebille, Z. Phys. A **340**, 63 (1991).

[2] M. Colonna, N. Colonna, A. Bonasera, and M. DiToro, Nucl. Phys. **A541**, 295 (1992).

[3] J. Suro, Y.D. Chan, J.A. Scarpaci, R.G. Stokstad, K. Möhring, and T.C. Schmidt, Nucl. Phys. **A548**, 353 (1992).

[4] R. Wada, M. Gonin, M. Gui, K. Hagel, Y. Lou, D. Utley, B. Xiao, D. Miller, J.B. Natowitz, D. Fabris, G. Nebbia, R. Zanon, B. Chambon, B. Cheynis, A. Demeyer, D. Drain, D. Guinet, X.C. Hu, C. Pastor, K. Zaid, J. Alarja, R. Bertholet, A. Giorni, A. Lleres, C. Morand, P. Stassi, L. Schussler, B. Viano, and P. Gonthier, Nucl. Phys. **A548**, 471 (1992).

[5] C. Schwarz, H. Fuchs, H. Homeyer, K. Möhring, T. Schmidt, A. Siwek, A. Sourell, W. Terlau, and A. Budzanowski, Z. Phys. A **345**, 29 (1993).

[6] G. Peilert, H. Stöcker, and W. Greiner, Rep. Prog. Phys. **57**, 533 (1994).

[7] H. Fuchs and K. Möhring, Rep. Prog. Phys. **57**, 231 (1994).

[8] S.P. Baldwin, B. Lott, B.M. Szabo, B.M. Quednau, W.U. Schröder, J. Tõke, L.G. Sobotka, J. Baretto, R.J. Charity, L. Gallamore, D.G. Sarantites, D.W. Stracener, and R.T. de Souza, Phys. Rev. Lett. **74**, 1299 (1995).

[9] Y. Larochelle, L. Beaulieu, G. Anctil, B. Djerroud, D. Doré, R. Laforest, J. Pouliot, R. Roy, M. Samri, C. St-Pierre, G.C. Ball, D.R. Bowman, A. Galindo-Uribarri, E. Hagberg, D. Horn, D. Guinet, and P. Lautesse, Phys. Rev. C **53**, 823 (1996).

[10] B. Lott, S.P. Baldwin, B.M. Szabo, B.M. Quednau, W.U. Schröder, J. Tõke, L.G. Sobotka, J. Barreto, R.J. Charity, L. Gallamore, D.G. Sarantites, and D.W. Stracener, Phys. Rev. Lett. **68**, 3141 (1992).

[11] B.M. Quednau, S.P. Baldwin, B. Lott, W.U. Schröder, B.M. Szabo, J. Tõke, D. Hilscher, U. Jahnke, H. Rossner, S. Bresson, J. Galin, D. Guerreau, M. Morjean, and D. Jacquet, Phys. Lett. B **309**, 10 (1993).

[12] J.F. Lecolley, L. Stuggé, M. Aboufirassi, A. Badala, B. Bilwes, R. Bougault, R. Brou, F. Cosmo, J. Colin, D. Durand, J. Galin, A. Genoux-Lubain, D. Guerreau, D. Horn, D. Jacquet, J.L. Laville, F. Lefebvres, C. LeBrun, J. Lemière, O. Lopez, M. Louvel, M. Mahi, M. Morjean, C. Paulot, A. Péghaire, N. Prot, G. Rudolf, F. Scheibling, J.C. Steckmeyer, B. Tamain, and S. Tomasevic, Phys. Lett. B **325**, 317 (1994).

[13] Y. Larochelle, G.C. Ball, L. Beaulieu, B. Djerroud, D. Doré, A. Galindo-Uribarri, P. Gendron, E. Hagberg, D. Horn, E. Jalbert, R. Laforest, J. Pouliot, R. Roy, M. Samri, and C. St-Pierre, Phys. Lett. B **352**, 8 (1995).

[14] J. Péter, S.C. Jeong, J.C. Angélique, G. Auger, G. Bizard, R. Brou, A. Buta, C. Cabot, Y. Cassagnou, E. Crema, D. Cussol, D. Durand, Y. El Masri, P. Eudes, Z.Y. He, A. Kerambrun, C. Lebrun, R. Legrain, J.P. Patry, A. Péghaire, R. Régimbart, E. Rosato, F. Saint-Laurent, J.C. Steckmeyer, B. Tamain, and E. Vient, Nucl. Phys. **A593**, 95 (1995).

[15] L. Beaulieu, Y. Larochelle, L. Gingras, G.C. Ball, D.R. Bowman, B. Djerroud, D. Doré, A. Galindo-Uribarri, D. Guinet, E. Hagberg, D. Horn, R. Laforest, P. Lautesse, R. Roy, M. Samri, and C. St-Pierre, Phys. Rev. Lett. **77**, 462 (1996).

[16] C.P. Montoya, W.G. Lynch, D.R. Bowman, G.F. Peaslee, N. Carlin, R.T. de Souza, C.K. Gelbke, W.G. Gong, Y.D. Kim, M.A. Lisa, L. Phair, M.B. Tsang, J.B. Webster, C. Williams, N. Colonna, K. Hanold, M.A. McMahan, G.J. Wozniak, and L.G. Moretto, Phys. Rev. Lett. **73**, 3070 (1994).

[17] J. Tõke, B. Lott, S.P. Baldwin, B.M. Quedneau, W.U. Schröder, L.G. Sobotka, J. Barreto, R.J. Charity, D.G. Sarantites, D.W. Stracener, and R.T. de Souza, Phys. Rev. Lett. **75**, 2920 (1995).

[18] J.F. Lecolley, L. Stuggé, M. Aboufirassi, B. Bilwes, R. Bougault, R. Brou, F. Cosmo, J. Colin, D. Durand, J. Galin, A. Genoux-Lubain, D. Guerreau, D. Horn, D. Jacquet, J.L. Laville, F. Lefebvres, C. Le Brun, O. Lopez, M. Louvel, M. Mahi, C. Meslin, M. Morjean, A. Péghaire, G. Rudolf, F. Scheibling, J.C. Steckmeyer, B. Tamain, and S. Tomasevic, Phys. Lett. B **354**, 202 (1995).

[19] G.D. Westfall, J. Gosset, P.J. Johansen, A.M. Poskanzer, W.G. Meyer, H.H. Gutbrod, A. Sandoval, and R. Stock, Phys. Rev. Lett. **37**, 1202 (1976).

[20] R. Stock, Phys. Rep. **135**, 259 (1986).

[21] B. Borderie, M.F. Rivet, and L. Tassan-Got, Ann. Phys. (Paris) **15**, 287 (1990).

[22] C.A. Pruneau, G.C. Ball, E. Hagberg, D. Horn, S. Gilbert, L. Potvin, C. Rioux, C. St-Pierre, T.E. Drake, A. Galindo-Uribarri, G. Zwartz, D.A. Cebra, S. Howden, J. Karn, C.A. Ogilvie, A. Vander Molen, G.D. Westfall, W.K. Wilson, and J.S. Winfield, Nucl. Phys. **A534**, 204 (1991).

[23] J.P. Alard, Z. Basrak, N. Bastid, I.M. Belayev, M. Bini, Th. Blaich, R. Bock, A. Buta, R. Čaplar, C. Cerruti, N. Cindro, J.P. Coffin, M. Crouau, P. Dupieux, J. Erö, Z.G. Fan, P. Fintz, Z. Fodor, R. Freifelder, L. Fraysse, S. Frolov, A. Gobbi, Y. Grigorian, G. Guillaume, N. Herrmann, K.D. Hildenbrand, S. Hölbling, O. Houari, S.C. Jeong, M. Jorio, F. Jundt, J. Kecskemeti, P. Koncz, Y. Korchagin, R. Kotte, M. Krämer, C. Kuhn, I. Legrand, A. Lebedev, C. Maguire, V. Manko, T. Matulewicz, G. Mgebrishvili, J. Mösner, D. Moisa, G. Montarou, P. Morel, W. Neubert, A. Olmi, G. Pasquali, D. Pelte, M. Petrovici, G. Poggi, F. Rami, W. Reisdorf, A. Sadchikov, D. Schüll, Z. Seres, B. Sikora, V. Simion, S. Smolyankin, U. Sodan, N. Taccetti, K. Teh, R. Tezkratt, M. Trzaska, M.A. Vasiliev, P. Wagner, J.P. Wessels, T. Wienold, Z. Wilhelmi, D. Wohlfarth, and A.V. Zhilin, Phys. Rev. Lett. **69**, 889 (1992).

[24] L. Stuttgé, J.C. Adloff, B. Bilwes, R. Bilwes, F. Cosmo, M. Glaser, G. Rudolf, F. Scheibling, R. Bougault, J. Colin, F. Delaunay, A. Genoux-Lubain, D. Horn, C. le Brun, J.F. Lecolley, M. Louvel, J.C. Steckmeyer, and J.L. Ferrero, Nucl. Phys. **A539**, 511 (1992).

[25] G. F. Bertsch and S. Das Gupta, Phys. Rep. **160**, 190 (1988).

[26] J. Aichelin and H. Stöcker, Phys. Lett. B **176**, 14 (1986).

[27] C. Pruneau, D. Horn, M.G. Steer, R.B. Walker, T. Whan, C. Rioux, R. Roy, C. St-Pierre, T.E. Drake, and A. Galindo-Uribarri, Nucl. Instrum. Methods Phys. Res. A **297**, 404 (1990).

[28] Y. Larochelle, L. Beaulieu, B. Djerroud, D. Doré, P. Gendron, E. Jalbert, R. Laforest, J. Pouliot, R. Roy, M. Samri, and C. St-Pierre, Nucl. Instrum. Methods Phys. Res. A **348**, 167 (1994).

[29] L. Beaulieu, Ph.D. thesis, Université Laval, 1996.

[30] H. Morgenstern, W. Bohne, W. Galster, K. Grabisch, and A. Kyanowski, Phys. Rev. Lett. **52**, 1104 (1984).

[31] N. Colonna, R.J. Charity, D.R. Bowman, M.A. McMahan, G.J. Wozniak, L.G. Moretto, G. Guarino, A. Pantaleo, L. Fiore, A. Gobbi, and K.D. Hildenbrand, Phys. Rev. Lett. **62**, 1833 (1989).

[32] K. Hagel, A. Péghaire, G.M. Jin, D. Cussol, H. Doubre, J. Péter, F. Saint-Laurent, G. Bizard, R. Brou, M. Louvel, J.P. Patry, R. Regimbart, J.C. Steckmeyer, B. Tamain, Y. Cassagnou, R. Legrain, C. Lebrun, E. Rosato, R.L. McGrath, S.C. Jeong, S.M. Lee, Y. Nagashima, T. Nakagawa, M. Ogihara, J. Kasagi, and T. Motobayashi, Phys. Lett. B **229**, 20 (1989).

[33] Y. Blumenfeld, N. Colonna, P. Roussel-Chomaz, D.N. Delis, K. Hanold, J.C. Meng, G.F. Peaslee, Q.C. Sui, G.J. Wozniak, L.G. Moretto, B. Libby, A.C. Mignerey, G. Guarino, N. Santoruvo, and I. Iori, Phys. Rev. Lett. **66**, 576 (1991).

[34] A. Malki, J.P. Coffin, G. Guillaume, F. Jundt, K. Krishan, F. Rami, P. Wagner, P. Fintz, M. Zahar, M. Gonin, B. Heusch, M. Ohta, B. Rastegar, D. Rebreyend, F. Merchez, J. Mistretta, and S. Kox, Z. Phys. A **339**, 283 (1991).

[35] G. Nebbia, J.A. Ruiz, D. Fabris, G. Viesti, R.H. Burch, F. Gramegna, G. Prete, A. Giorni, A. Lleres, J.B. Viano, B. Chambon, B. Cheynis, A. Demeyer, D. Drain, D. Guinet, X.C. Hu, M. Gonin, K. Hagel, J.B. Natowitz, R. Wada, and P.L. Gonthier, Phys. Rev. C **45**, 317 (1992).

[36] K. Hanold, L.G. Moretto, G.F. Peaslee, G.J. Wozniak, D.R. Bowman, M.F. Mohar, and D.J. Morissey, Phys. Rev. C **48**, 723 (1993).

[37] S. Datta, K. Krishan, and S. Bhattacharya, Z. Phys. A **353**, 49 (1995).

[38] J.A. Scarpaci, Y. Chan, D. DiGregorio, B.A. Harmon, J. Pouliot, R.G. Stokstad, and J. Suro, Phys. Rev. C **52**, 764 (1995).

[39] D. Durand, Nucl. Phys. **A541**, 266 (1992).

[40] H. Ströbele, R. Brockmann, J.W. Harris, F. Riess, A. Sandoval, R. Stock, K.L. Wolf, H.G. Pugh, L.S. Schroeder, R.E. Renfordt, K. Tittel, and M. Maier, Phys. Rev. C **27**, 1349 (1983).

[41] J. Cugnon and D. L'Hote, Nucl. Phys. **A397**, 519 (1983).

[42] N. Cindro, M. Korolija, E. Běták, and J.J. Griffin, Phys. Rev. Lett. **66**, 868 (1991).

[43] A. Hakim, A. Fahli, M. Ohta, G. Guillaume, J.P. Coffin, P. Fintz, J. Jundt, A. Malki, F. Rami, B. Rastegar, P. Wagner, and M. Zahar, Nuovo Cimento A **107**, 1587 (1994).

[44] W. Bauer and A. Botvina, Phys. Rev. C **52**, R1760 (1995).

[45] C. Brusati, M. Cavinato, E. Fabrici, E. Gadioli, and E. Gadioli-Erba, Z. Phys. A **353**, 57 (1995).

[46] J.F. Dempsey, R.J. Charity, L.G. Sobotka, G.J. Kunde, S. Gaff,

C.K. Gelbke, T. Glasmacher, M.J. Huang, R.C. Lemmon, W.G. Lynch, L. Manduci, L. Martin, M.B. Tsang, D.K. Agnihotri, B. Djerroud, W.U. Schröder, W. Skulski, J. Tõke, and W.A. Friedman, Phys. Rev. C **54**, 1710 (1996).
[47] T.C. Awes, S. Saini, G. Poggi, C.K. Gelbke, D. Cha, R. Legrain, and G.D. Westfall, Phys. Rev. C **25**, 2361 (1982).
[48] Z. Saddiki, Master's thesis, Université Laval, 1996.
[49] M. Blann and B. Remington, Phys. Rev. C **37**, 2231 (1988).
[50] J.P. Wieleczko, E. Plagnol, and P. Ecomard, in *Proceedings of the 2nd TAPS Workshop 1994*, edited by Martinez Diaz and Guardemar Schutz (World Scientific, Singapore, 1995), p. 145.
[51] R. Laforest, Ph.D. thesis, Université Laval, 1994.
[52] D. Doré, Ph.D. thesis, Université Laval, 1994.
[53] A. Lleres, A. Giorni, H. Elhage, M.E. Brandan, A.J. Cole, P. Désesquelles, D. Heuer, A. Menchaca-Rocha, J.B. Viano, F. Benrachi, B. Chambon, B. Cheynis, D. Drain, and C. Pastor, Phys. Rev. C **48**, 2753 (1993).
[54] C.H. Dasso and G. Pollarolo, Comput. Phys. Commun. **50**, 341 (1988).
[55] R.J. Charity, M.A. McMahan, G.J. Wozniak, R.J. McDonald, L.G. Moretto, D.G. Sarantites, L.G. Sobotka, G. Guerino, A. Pantaleo, L. Fiore, A. Gobbi, and K.D. Hildenbrand, Nucl. Phys. **A483**, 371 (1988).
[56] J.A. López and J. Randrup, Comput. Phys. Commun. **70**, 92 (1990).
[57] W. Bauer, G. F. Bertsch, W. Cassing, and U. Mosel, Phys. Rev. C **34**, 2127 (1986).
[58] L. Sobotka, Phys. Rev. C **50**, R1772 (1994).
[59] M. Colonna, M. Di Toro, and A. Guarnera, Nucl. Phys. **A589**, 160 (1995).
[60] J. Aichelin, Phys. Rep. **202**, 233 (1991).
[61] C. Dorso and J. Randrup, Phys. Lett. B **215**, 611 (1988).
[62] G. Peilert, J. Konopka, H. Stöcker, W. Greiner, M. Blann, and M. G. Mustafa, Phys. Rev. C **46**, 1404 (1992).
[63] Toshiki Maruyama, Akira Ohnishi, and Hisashi Horiuchi, Phys. Rev. C **42**, 386 (1990).
[64] Toshiki Maruyama, Akira Ohnishi, and Hisashi Horiuchi, Phys. Rev. C **45**, 2355 (1992).